Rydberg-Raman-Ramsey resonances in atomic vapor

Rob Behary,[1] Alex Gill,[2] Aaron Buikema,[2] Eugeniy E. Mikhailov,[1] and Irina Novikova[1]
[1]*Department of Physics, William & Mary, Williamsburg, Virginia 23187, USA*
[2]*The Charles Stark Draper Laboratory, Inc., Cambridge, Massachusetts 02139, USA*

(Received 13 October 2023; accepted 22 April 2024; published 6 May 2024)

The sensitivity of electric field sensors based on two-photon electromagnetically induced transparency (EIT) involving highly excited Rydberg states in thermal atoms is often limited by the residual Doppler effect and optical power broadening. Here, we propose a method to reduce the EIT spectral linewidth using a Ramsey interrogation approach, allowing multiple interrogations of atomic coherence, using either temporally or spatially separated laser beams. Our theoretical calculations predict that the linewidth of such Raman-Ramsey spectral features can be substantially reduced compare to a standard Doppler-broadened EIT, opening a possibility to improve sensitivity of Rydberg atomic vapor-based sensors.

DOI: 10.1103/PhysRevA.109.053706

I. INTRODUCTION

The application of atomic vapor cells for precision optical measurements and sensing has a long and successful history. Electromagnetically induced transparency (EIT) [1–4] enables a convenient link between optical transmission and minute variations in atomic energy levels caused by, e.g., external electromagnetic fields. Rydberg EIT in atomic vapors [5,6] has already become a well established method for in situ measurements of dc and rf electric fields [7–11], development of broadband rf receivers and analyzers [12–14], THz imaging [15–17], SI-traceable electric field standards [18], etc. However, power broadening and thermal atomic motion ultimately limit the width and amplitude of the observable EIT peak, deteriorating its achievable sensitivity.

In this paper, we theoretically investigate the possibility to overcome these limitations and obtain significantly narrower spectral resonances by using a Raman-Ramsey approach, in which optical interrogation of atoms is interrupted by evolution in the dark. We consider two possible scenarios: temporal separation, which uses two bichromatic optical pulses to first prepare and then read out atomic coherence between the ground and Rydberg states, as shown in Fig. 1(a); and spatial separation, where moving atoms encounter two separate interaction regions of continuous optical fields, shown in Fig. 1(b). We find that in either case a narrow Rydberg-Raman-Ramsey (R^3) spectral feature emerges in addition to the standard Rydberg EIT peak. Since only slow atoms can constructively contribute to formation of R^3 resonances, the effect of the residual Doppler broadening is significantly reduced. In what follows, we present a theoretical model describing the R^3 signal for both time- and space-separated Ramsey interactions, and analyze the effect of atomic motion. Our model predicts that R^3 spectroscopy may provide superior sensitivity to the Rydberg level energy shifts, despite its reduced amplitude.

II. THEORETICAL MODEL

In this section we briefly summarize the three-level interaction model used to describe dynamic changes in the Rydberg EIT system shown in Fig. 2(a) for stationary atoms. In this model, two optical laser fields (a *probe* and a *coupling*) interact with corresponding atomic optical transitions, and the transmission of the probe beam is measured. The probe field with Rabi frequency Ω_P couples the ground state $|g\rangle$ with the first intermediate excited electron state $|e\rangle$, the population of which decays with a rate Γ_e (in our system this is the $5S_{1/2}F = 3 \rightarrow 5P_{3/2}F'$ optical transition in ^{85}Rb). Simultaneously, the coupling laser (Rabi frequency Ω_C) couples state $|e\rangle$ to a Rydberg state $|r\rangle$ with significantly smaller decay rate Γ_r (in our case $|r\rangle$ is the ^{85}Rb $45D_{5/2}$ state, $1/\Gamma_r \approx 50$ μs). Using standard dipole and rotating wave approximations, the interaction Hamiltonian of the system can be written as [19–21]

$$\hat{H} = \frac{\hbar}{2}\begin{pmatrix} 0 & \Omega_P^* & 0 \\ \Omega_P & -2\Delta_P & \Omega_C^* \\ 0 & \Omega_C & -2(\Delta_P + \Delta_C) \end{pmatrix}, \tag{1}$$

where $\Delta_{P,C}$ are the values of the one-photon detuning of each laser from the corresponding optical transitions. For now, we assume motionless atoms and discuss the effect of their thermal motion in the following sections.

To simulate the evolution of the atomic parameters, we use the Lindblad master equation:

$$\frac{\partial \rho}{\partial t} = -\frac{i}{\hbar}[\hat{H}, \rho] + \sum_i \hat{\mathcal{L}}(\rho, \sigma_i), \tag{2}$$

where $\hat{\mathcal{L}}$ is the Lindblad superoperator given by $\mathcal{L}(\rho, \hat{\sigma}_i) = \sum_i \hat{\sigma}_i \rho \hat{\sigma}_i^\dagger - (\hat{\sigma}_i^\dagger \hat{\sigma}_i \rho + \rho \hat{\sigma}_i^\dagger \hat{\sigma}_i)/2$, and $\hat{\sigma}_i$ are the collapse operators that account for the decoherence mechanisms. For our interaction system, we include the Lindblad superoperator $\hat{\mathcal{L}}_D$ for atomic decays which can be written as

$$\hat{\mathcal{L}}_D = \begin{pmatrix} \Gamma_e \rho_{ee} & -\frac{\Gamma_e}{2}\rho_{ge} & -\frac{\Gamma_r}{2}\rho_{gr} \\ -\frac{\Gamma_e}{2}\rho_{eg} & -\Gamma_e \rho_{ee} + \Gamma_r \rho_{rr} & -\frac{(\Gamma_e+\Gamma_r)}{2}\rho_{er} \\ -\frac{\Gamma_r}{2}\rho_{rg} & -\frac{(\Gamma_e+\Gamma_r)}{2}\rho_{re} & -\Gamma_r \rho_{rr} \end{pmatrix}. \tag{3}$$

 ©2024 American Physical Society

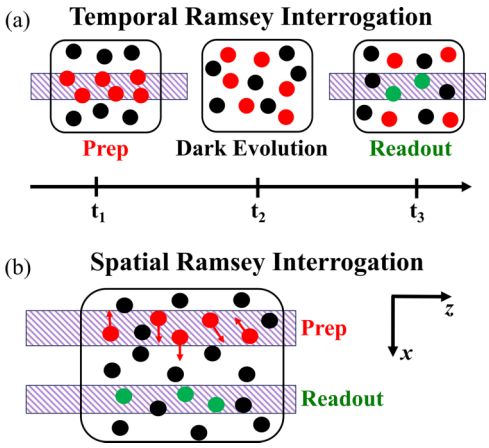

FIG. 1. (a) *Temporal* R^3 *resonances:* Atoms are prepared in the coherent superposition with two EIT laser fields (red) during time t_1, and then allowed to evolve in the dark for time t_2, while laser fields are turned off. Any changes in the atomic coherence are read out with a second light pulse (containing both EIT laser fields) of duration t_3. Only the initially prepared atoms remaining in the interaction volume (green) contribute to the R^3 resonance. (b) *Spatial* R^3 *resonances:* Atoms are prepared in the coherent superposition with two EIT laser fields (red) in a preparation interaction region, and move ballistically toward the readout region (also containing two EIT laser fields), crossing the dark region in between. Only the atoms reaching the readout region (green) contribute to the R^3 resonance formation.

Coherent EIT excitation assumes constant phase between the probe and coupling lasers, and thus in practice the lifetime of the atomic coherence between the ground and the most excited level is limited by the relative coherence of these laser fields. The Lindblad superoperator $\hat{\mathcal{L}}_{lw}$ accounts for the finite width of the probe and coupling laser fields γ_P and γ_C, respectively:

$$\hat{\mathcal{L}}_{lw} = \begin{pmatrix} 0 & -\gamma_P\rho_{ge} & -(\gamma_P+\gamma_C)\rho_{gr} \\ -\gamma_P\rho_{eg} & 0 & -\gamma_C\rho_{er} \\ -(\gamma_P+\gamma_C)\rho_{rg} & -\gamma_C\rho_{re} & 0 \end{pmatrix}. \quad (4)$$

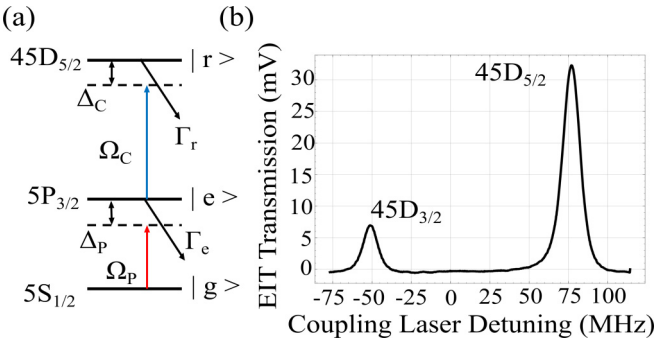

FIG. 2. (a) Three-level ladder system with ground state $|g\rangle$, intermediate excited state $|e\rangle$, and Rydberg state $|r\rangle$ in ^{85}Rb. Probe laser with Rabi frequency Ω_P couples $|g\rangle$ and $|e\rangle$, while a coupling laser with Rabi frequency Ω_C couples $|e\rangle$ and $|r\rangle$. Δ_P and Δ_C are the detunings of the probe and coupling lasers respectively. (b) An example experimental EIT spectrum, showing probe transmission as a function of the coupling laser detuning.

Solving Eq. (2) for the matrix element ρ_{ge}, we find expressions for the complex optical susceptibility $\chi(\Delta_P, \Delta_C)$ of the probe optical field, the absorption coefficient α, and the refractive index n:

$$\chi(\Delta_P, \Delta_C) = -\frac{2\mathcal{N}|\mathbf{d}_{ge}|^2}{\hbar\epsilon_0\Omega_P}\rho_{eg} \quad (5a)$$

$$\alpha = k_P\,\mathrm{Im}[\chi] \quad (5b)$$

$$n = 1 + \mathrm{Re}[\chi]/2, \quad (5c)$$

where $\mathcal{N}$ is the atomic number density, $\mathbf{d}_{ge}$ is the dipole moment of the $|g\rangle$-$|e\rangle$ atomic transition, and $k_P = 2\pi/\lambda_P$ is the wave number of the probe optical field.

In the steady-state limit, one can easily reproduce the standard EIT resonance in the probe field transmission, similar to the experimental example shown in Fig. 2(b). In cold atoms, the width of such EIT peak is ultimately limited by the lifetime of the ground-Rydberg state coherence and potentially by the linewidth of the lasers $(\gamma_P + \gamma_C)^{-1}$, and can be very narrow (a few kHz), but increases linearly with laser power. For practical applications it is advantageous to use a somewhat power-broadened EIT resonance, as higher laser power provides more efficient coherence preparation and thus higher EIT resonance amplitude, as well as reduces the relative effect of the photon shot noise.

To reduce the effect of the power broadening without compromising the advantages of stronger probe optical field, we propose to use the Raman-Ramsey interrogation scheme, consisting of two relatively strong laser pulses separated by a "dark" time, as shown in Fig. 1(a). Such Raman-Ramsey interrogation schemes have been successfully implemented for improving the performance of the atomic clocks based on Λ-based EIT systems [22,23]. In this case, atoms are first prepared in the desired coherent superposition of the ground and Rydberg atomic states using the first optical pulse, consisting of both EIT laser fields. Then the laser fields are quickly turned off, and the long-lived coherence between the ground and the Rydberg state ρ_{gr} is allowed to evolve in the dark for time $1/\Gamma_r \geqslant t_2 \geqslant 1/\Gamma_e$. During this evolution its phase is affected by any perturbation in the Rydberg state energy, and can be later read out using the second (detection) laser pulse whose power and duration can be optimize to achieve the highest signal-to-noise ratio. Most importantly, since most of the coherent evolution happens in the absence of interaction with optical fields, the effect of the power broadening is greatly reduced, even if strong fields are used in the preparation and detection stages.

We calculate all atomic state evolution using the Python package QUTIP [24], following the time sequence shown in Fig. 3(a). To simplify the calculations, we assume that the preparation time t_1 is long enough for the system to reach the steady state for the given initial laser parameters. For the dark evolution time $t_2 \gg 1/\Gamma_e$, the population of the intermediate excited state and the coherence between the ground state and intermediate excited state quickly vanish. On the other hand, the population of the Rydberg state ρ_{rr} and the coherence between ground and Rydberg states ρ_{gr} survive, as they decay much slower, and we can take advantage of this consideration to simplify the model by replacing the exact numerical simulations for all atomic parameters at the end of the dark

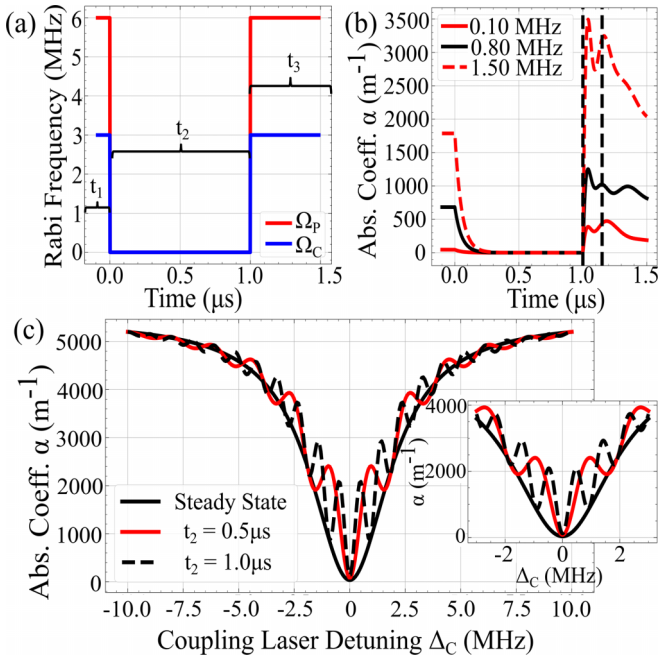

FIG. 3. (a) Time sequence of temporal Ramsey interrogation for stationary atoms. (b) Theoretically predicted R^3 optical response for stationary atoms for different two-photon detunings δ_R. Black dashed lines indicate the 150 ns integration region used to reconstruct Ramsey fringes. (c) R^3 resonances as a function of the coupling laser detuning for different evolution in the dark time t_2. The model parameters are $\Delta_P = 0, \Gamma_e = 6\,\text{MHz} \times 2\pi, \Gamma_r = 3\,\text{kHz} \times 2\pi, \Omega_C = 0.5\Gamma_e, \Omega_P = \Gamma_e, \mathcal{N} = 1.7 \times 10^{11}\ \text{cm}^{-3}, \mathbf{d}_{ge} = 1.46 \times 10^{-29}\ \text{C m}$.

evolution with simple analytical solutions for nonvanishing coherences:

$$\rho_{rr} = \rho_{rr,ss} e^{-t_2\Gamma_r}, \tag{6a}$$

$$\rho_{gg} = 1 - \rho_{rr}, \tag{6b}$$

$$\rho_{gr} = \rho_{gr,ss} e^{-\frac{\Gamma_r}{2}t_2} e^{-i(\Delta_C+\Delta_P)t_2}. \tag{6c}$$

In Eq. (6), $\rho_{rr,ss}$ and $\rho_{gr,ss}$ refer to the steady state solution of the density matrix before the dark time. In the case of nonzero two-photon detuning $\delta_R = \Delta_C + \Delta_P \neq 0$, ρ_{gr} acquires a phase $e^{i\delta_R t_2}$. Finally, using the density matrix with only nonzero ρ_{gg}, ρ_{rr}, and ρ_{gr} as the initial conditions, we numerically solve the Lindblad master equation in time for a fixed detection time t_3. The simulated time response of different coupling laser detunings is shown in Fig. 3(b). Dotted vertical black lines in Fig. 3(b) show the region the atomic response is integrated over to produce R^3 resonances. If this time is shorter than the time required to reestablish the steady-state EIT, the probe laser transmission is largely determined by the accumulated phase of ρ_{gr}, and displays a clear interference-like fringe pattern, as shown in Fig. 3(c) with the frequency inversely proportional to the dark evolution time. Thus we can theoretically achieve the spectral resolution limited only by the Rydberg state decoherence time.

III. EFFECT OF ATOMIC MOTION ON THE R^3 RESONANCES

The motion of atoms in thermal atomic vapor greatly affects the characteristics of two-photon optical resonances. For temporal Raman-Ramsey excitation, we only consider atomic motion in the $+z$ direction of the laser propagation. The transverse size of the laser beam in this case mainly limits the interaction time and effectively reduces the Rydberg state lifetime. The longitudinal motion of atoms produces two generally undesirable effects on the R^3 fringe formation, both related to the large frequency mismatch between two optical fields. The first one is the spatial phase variation between the probe and coupling fields, and the other is the differential Doppler shift for atoms with different longitudinal velocities.

We consider the Doppler effect first, as it equally affects R^3 and steady-state EIT resonances, and has been identified as one of the main limiting factors for Rydberg EIT-based sensor sensitivity. If an atom moves with velocity v_z along the laser beam, it "sees" the laser frequency ω shifted by $\omega v_z/c$. Even in the most beneficial geometry of the counterpropagating beams, that creates a large velocity-dependent variation in the two-photon detuning $\delta_R(v_z) = (\Delta_C + \Delta_P - \omega_{rg}) + (k_P - k_C)v_z$. Practically, it means that even if the lasers are tuned precisely to the two-photon resonance, only a relatively small fraction of atoms with near-zero longitudinal velocities contribute to the EIT formation, and that the observable EIT linewidth is broadened by this residual Doppler effect to a few MHz. In the case of Raman-Ramsey excitation, such Doppler mismatch makes the phase acquired during the dark evolution dependent on atomic velocity. This results in a relative shift of the Ramsey fringes for each velocity group, as shown in Fig. 4(a). If this effect is considered in isolation, it can wash away the fringes almost completely when the transmission is integrated over all velocity classes.

We also need to take into account the spatial variation of the relative phase of the two optical fields along the beam path. The initial phase of ρ_{gr} is set by the relative phase of Ω_C and Ω_P. Due to the mismatch in wave vectors, this phase is position-dependent, so if an atom moves between the preparation and detection steps, the phase of the R^3 fringe reflects this phase difference.

This effect almost exclusively affects R^3 fringe formation, rather than steady-state EIT, since in the latter case the coherence phase adiabatically adjusts as atoms move along the laser beams. However, in the Raman-Ramsey process, moving atoms, detected at $z = 0$, have been prepared at the location $-v_z t_2$, and thus their coherent state carries an additional phase $-(k_P - k_C)v_z t_2$ (for the counterpropagating optical fields). Again, the contributions of different velocity groups destructively interfere, in principle limiting the fraction of atoms that can contribute to the observation of R^3 resonance. Figure 4(b) shows the fringe shifts due to the spatial phase mismatch for different v_z. However, when considered together, these two phase shifts partially compensate each other. Figure 4(c) shows that the Doppler effect and relative displacement effects work together to bring the fringes back to constructive interference and preserve narrow fringes. Thus, R^3 fringes "survive" the integration of the one-dimensional (1D) Maxwell-Boltzmann velocity distribution of atoms in the

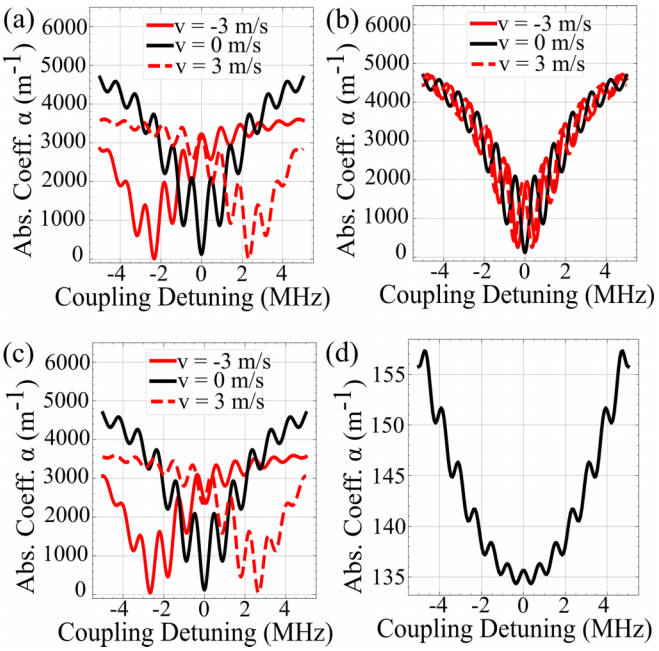

FIG. 4. Examples of Ramsey fringe modifications for longitudinal motion of atoms ($\hat{z}$). For (a)–(c) it is assumed that all atoms move with the given velocities v_z to illustrate the effects of phase and Doppler mismatch. (a) Effect of Doppler mismatch of detunings. (b) Effect of spatial phase variations. (c) Effect of both Doppler and phase variations. (d) Fringes resulting from dark time $t_2 = 1$ μs and $t_3 = 150$ ns for a range of velocities integrated over a thermal 1D distribution corresponding to 300 K; note the different scale for α.

z direction, as shown in Fig. 4(d) for a single t_2 dark time, albeit with reduced amplitude compared to the cold atom case due to fewer participating atoms.

IV. REALIZATION OF R^3 RESONANCES USING TWO SPATIALLY SEPARATED REGIONS

This analysis gives a somewhat optimistic outlook on the possibility of observing narrower Rydberg EIT features using Raman-Ramsey excitation. However, from the practical point of view, such temporal interrogation may introduce some technical complications, such as the need for excellent pulse synchronization, fast pulse turn on and turn off, and a low detection duty cycle. An alternative approach for taking advantage of the same effect with steady-state lasers is implementing spatially separated preparation and detection regions. In this case, the dark time occurs naturally when atoms fly between the two interaction regions. Several geometries of such spatial multiregional interaction have been tested previously for a Λ-type EIT systems [25–27].

To properly describe the atomic response for the spatial version of R^3 resonances, we can assume two parallel interaction regions, separated by the gap, as shown in Fig. 1(b). To increase the number of interacting atoms, we assume that both regions are stretched in the perpendicular direction. In this case, it is sufficient to consider the 2D motion of atoms between the two interaction regions as shown in Fig. 5(a). We assume that an atom first interacts with two laser fields in the preparation region long enough to reach the steady state.

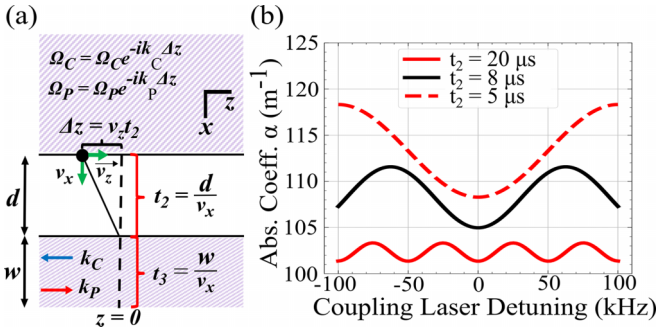

FIG. 5. (a) Spatially separated geometry model. Each interaction region (purple) contains counterpropagating probe and coupling beams. The preparation region (top) is assumed sufficiently wide, and separated by distance d from the detection region that has a finite width w. (b) Examples of Ramsey fringes for atoms with different transverse velocities v_x (resulting in different effective dark times t_2) integrated over the longitudinal velocities v_z.

Atoms with nonzero transverse velocity v_x eventually leave the preparation region and travel toward the detection region, effectively recreating the time sequence explored before and shown in Fig. 3(a). For each group of atoms with transverse velocity v_x the effective evolution in the dark time is $t_2 = d/v_x$, where d is the distance between the two interaction regions. As a result, atoms moving with different transverse velocities produce Ramsey fringes with different periods, as shown in Fig. 5(b). The fringes are also integrated over a range of thermal velocities in the z direction in order to capture the effect of phase shifts due to relative displacement. The central fringe survives when contributions of all velocity classes in both dimensions are integrated.

Figure 6(a) shows a theoretically predicted R^3 resonance, calculated using the same atomic parameters as Fig. 3 with a beam separation of $d = 1$ mm and a second interaction region of width $w = 50$ μm. Here we integrate the contributions to the optical susceptibility from each longitudinal velocity class for a given dark time t_2, and then integrate these results over all possible dark times $t_2 = d/v_x$. Because of the mutually destructive contributions of atoms with different velocities, we carefully optimized number of velocity classes included in the simulations. For the longitudinal integration, the simulated density matrix element reaches a stable point at an integration range of $-6 \leqslant \Delta z \leqslant 6$ μm with 75 included velocity classes. For the transverse integration range we use $0 \leqslant v_x \leqslant 400$ m/s with 50 velocity classes. These limits not only help manage simulation run time but also show the integrated signal is not a product of numerical instability.

The resulting optical absorption in Fig. 6(a) clearly shows two spectral features of different widths. The broader resonance is a "standard" Doppler-broadened EIT resonance due to atoms interacting with light only in the detection region. However, the second interaction for slower atoms produces an additional narrow feature on top of the broad EIT resonance: the R^3 resonance. The details of this narrow spectral features are best shown in Fig. 6(b). The full-width at half maximum (FWHM) of the resulting resonance is quite narrow, near 120 kHz, which is almost two orders of magnitude narrower than the broad EIT feature, even though its amplitude is

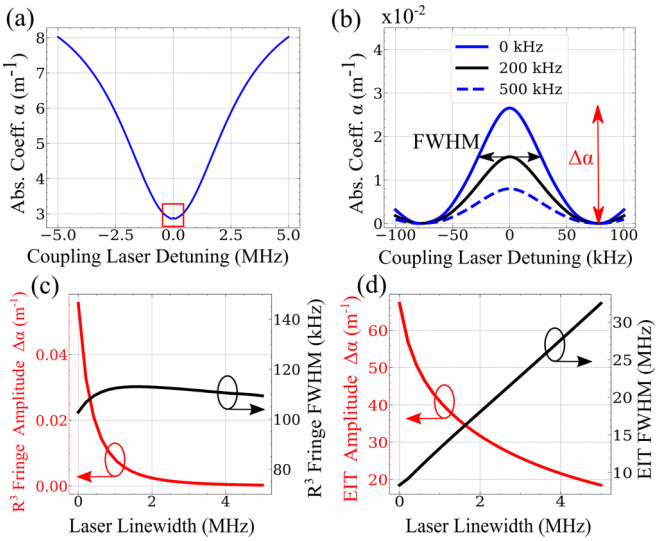

FIG. 6. (a) Predicted R^3 absorption resonance as a function of coupling laser detuning for $d = 1$ mm and $w = 50$ μm. The red box is the zoomed scale for the traces in (b). (b) The narrow R^3 feature for laser linewidths of the probe and coupling lasers at 0, 200, and 500 kHz. (c) Amplitude and FWHM of the R^3 feature for increasing laser linewidths. (d) Amplitude and FWHM of standard Doppler-broadened EIT for increasing laser linewidths.

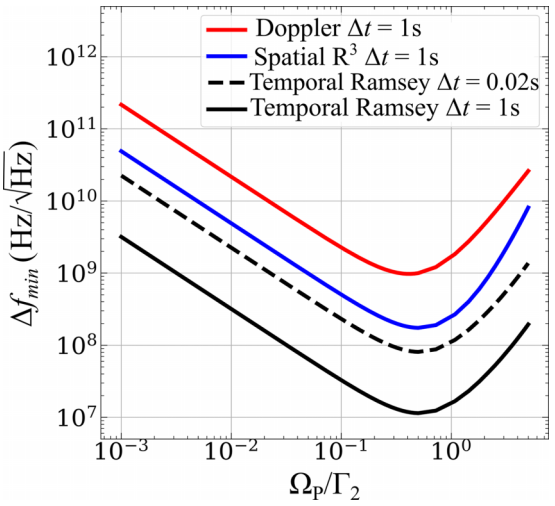

FIG. 8. Comparison of the minimum detectable frequency shift between standard Doppler-broadened EIT, spatially separated R^3, and temporally separated Ramsey measurements. $\Delta f_{\min}$ is calculated as described in Eq. (7). Here the temporal Ramsey case is calculated with a different Δt detection time to account for the short integration time to produce the signal.

much smaller as well. What is remarkable is that this narrow linewidth is fairly immune to the finite laser linewidth. Figure 6(c) gives a more complete picture of the effect of the laser linewidths on the R^3 resonance. For this simulation the laser linewidths γ_C and γ_P are considered equal for simplicity, and have values of 0, 100 kHz, and 500 kHz. The FWHM of the fringe only increases in value from 116 kHz to 125 kHz, but its amplitude drops as the laser linewidth increases. This is not unexpected: only a fraction of atoms with intact coherence contribute to the detection of the Raman-Ramsey feature, while additional dephasing reduces the fraction of atoms participating in R^3 resonance formation. In contrast, the linewidth of the standard EIT resonance increases linearly with the laser detuning, as shown in Fig. 6(d).

Figure 7 shows the impact of interaction channel separation distance d on the FWHM and amplitude of this central fringe. Figure 7(a) demonstrates the evolution of the fringe as the separation distance d increases. Figure 7(b) shows the same

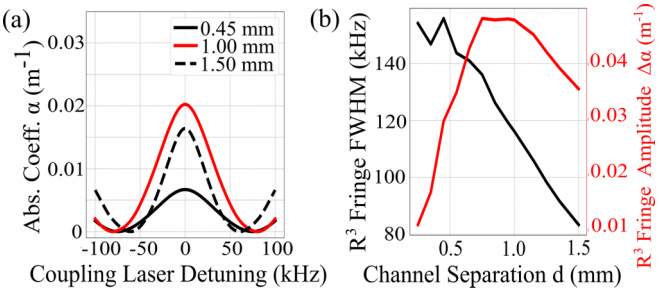

FIG. 7. Simulated central R^3 spatial fringes for varying measurement parameters. (a) R^3 fringe for various channel separation distances d. (b) Values for FWHM and height of the R^3 fringe vs. d.

analysis of the amplitude and FWHM as done for Fig. 6 but now as a function of separation distance d. As expected, we observe a reduction of resonance amplitude for larger channel separation; the height of the peak reaches its maximum value near $d = 1$ mm and then starts to decay, as fewer coherently prepared atoms survive the crossing between the two regions.

While we did not observe the R^3 fringe experimentally, preliminary experimental efforts testing the spatially separated geometry are detailed in the Appendix.

V. COMPARISON OF DIFFERENT INTERROGATION SCHEMES

To compare the potential advantage of a narrow R^3 resonance over standard single-interaction steady-state EIT, we have to choose a figure of merit for spectral resolution (or sensitivity). A small frequency variation Δf from the EIT peak due to an incident electric field produces a change in the probe transmission proportional to the first derivative of the spectral response vs coupling laser frequency. Assuming shot-noise limited measurements, we can then calculate the minimum detectable frequency change $\Delta f_{\min}$:

$$\Delta f_{\min} = \left[2L \frac{\partial \alpha}{\partial \Delta_C} \sqrt{\frac{P}{\hbar \omega}} \sqrt{\Delta t} \right]^{-1}, \tag{7}$$

where $L = 2.5$ cm is the interaction region length, P is the power of the probe laser for a given Ω_P, and Δt is the duration of the measurements. Figure 8 shows the

dependence of $\Delta f_{\min}$ as a function of increasing probe laser power for the different interrogation schemes at $\Delta t = 1$ s. It is clear that time-separated R^3 fringe should provide significantly higher sensitivity. However, such straightforward comparison gives it an unfair advantage for the temporally separated Ramsey case, since in reality only a small fraction (first 100 ns of the read-out pulse) of the time sequence is devoted to the data collection, since it takes $t_1 \approx 1$ μs to reach the steady-state EIT regime. Thus, assuming the dark time $t_2 = 1$ μs, the useful signal is collected only during 1/50 of the whole cycle. Thus, to properly compare the three different methods, we also include the sensitivity trace for the temporally separated Ramsey fringe case with $\Delta t = 0.02$ s.

A comparison of the $\Delta f_{\min}$ as a function of the probe Rabi frequency is shown in Fig. 8. Both Ramsey style measurements predict a smaller detectable frequency shift than the standard Doppler-broadened case. Thus, at least in the idealized case considered here, the method of spatially and temporally separated Ramsey fringes can lead to a more sensitive measurement.

VI. SUMMARY

In this paper we develop a model for Rydberg-Raman-Ramsey (R^3) EIT resonances by calculating the atomic response due to the repeated interactions with two optical fields in two-photon Raman resonances. We focused on the effect of the atomic motion on the resulting narrow spectral feature for spatially or temporally separated interaction regions. We predict that even for thermal atoms it should be possible to observe R^3 resonances in the temporal and spatially separated cases, even with the inclusion of decoherence mechanisms due to laser linewidths. We also show that using this resonance can potentially improve sensitivity to electric field measurements in a discussion of the minimum detectable frequency.

ACKNOWLEDGMENTS

This work was sponsored by the Defense Advanced Research Projects Agency under DARPA Program No. BAA HR001120S0048 "Defense Sciences Office Office-wide" issued by DARPA/CMO under Contract No. HR0011-22-C-0061.

APPENDIX: PRELIMINARY EXPERIMENTAL MEASUREMENTS

Here we present some preliminary experimental investigations of the spatially separated beam geometry using a two channel detection scheme as shown in Fig. 9(a). For these experiments, our coupling laser is tuned to resonance with the $5P_{3/2} \rightarrow 56D_{5/2}$ transition. Channels A and B refer to the two spatially separated optical interrogation regions, each containing one or both of the 780 nm probe or 480 nm coupling light propagating along the z direction. For this preliminary stage we did not have an ability to control relative phases of the optical fields in the two channels, and thus focused on observing the phase-independent Rydberg population transfer by independently monitoring the optical absorption in either probe beam.

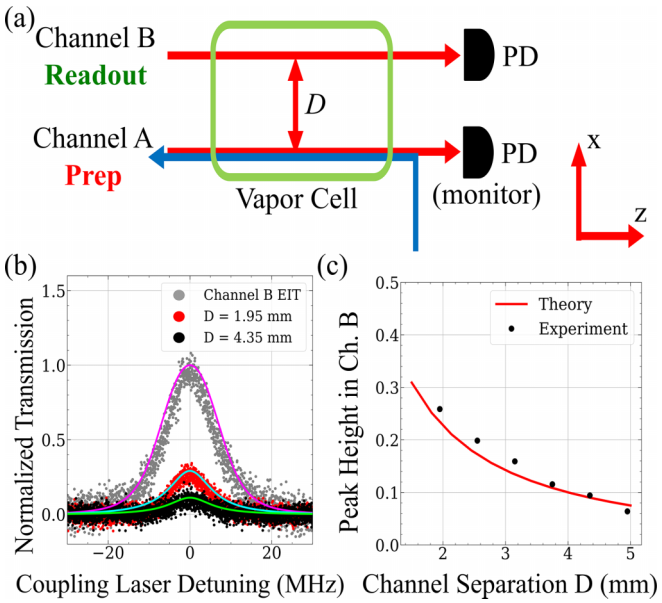

FIG. 9. (a) Experimental setup for spatially separated beam geometry. (b) The transmission of infrared light in channel B for a given beam separation D. Reported transmission is normalized to the peak steady-state EIT transmission experimentally observed using only the infrared and blue beams of channel B (channel A blocked) shown on the grey curve. Channel A and channel B EIT signals are similar when both red and blue lasers are present. Solid curves correspond to simulated spectra for the same parameters. (c) The experimentally measured EIT peak height as a function of beam separation, as compared with the results predicted by our theoretical model with no free parameters.

For these measurements we used oval-shaped laser beams. The sizes of the beams were the same in each channel with the probe beam diameters of 100 μm in the x direction and 8 mm in the y direction, and the coupling beam diameters of 100 μm in the x direction and 6 mm in the y direction. The manual adjustments of the separation distance D between the channel allowed us to explore the effect of this parameter on the probe transmission. Since residual optical interference between beams of the same color occurs for separation distances below $D \approx 0.5$ mm (as confirmed using a beam profiler placed at the position of the cell), we maintain sufficient channel separation to eliminate the effects of crosstalk between channels. We verified that there is negligible channel A probe light striking the channel B detector and vice versa. We also ensure that there is negligible overlap of channel A coupling light with the channel B probe, as evidenced by the lack of an observable EIT signal seen from just these two fields alone.

Using this setup we clearly observed the effects of the Rydberg atoms moving between the two interaction regions. For these measurements only atoms in channel A were excited to the steady-state Rydberg EIT state via the two-photon transition, while channel B contained only the 780 nm probe laser. Nevertheless, if the frequency of the 480 nm laser was varied in channel A across the EIT transmission peak, matching variation in the nominal probe absorption was detected, as shown in Fig. 9(b), indicating the presence of atoms prepared in a Rydberg-dressed dark state from channel A. In Fig. 9(c)

we show that as the channels are moved further apart, the detected EIT peak in channel B decreases in amplitude. This result is supported by the numerical model and is qualitatively explained by the correlation of larger values of D with higher average transverse speed v_x of the detected Rydberg atom population. Because the readout channel has a fixed width, a higher transverse speed results in a reduced readout interrogation time and a decrease in signal amplitude.

While this observation of the flight of room temperature Rydberg-dressed atoms between two channels is a necessary first step for spatially separated Ramsey interrogation, the setup is not yet optimized to achieve sufficient signal-to-noise ratio to observe a Ramsey fringe experimentally. Additionally, laser frequency and optical path-length stabilization concerns must be addressed in order to stabilize the anticipated Ramsey phase.

[1] S. E. Harris, Phys. Today **50**(7), 36 (1997).
[2] M. D. Lukin, Rev. Mod. Phys. **75**, 457 (2003).
[3] M. Fleischhauer, A. Imamoglu, and J. P. Marangos, Rev. Mod. Phys. **77**, 633 (2005).
[4] R. Finkelstein, S. Bali, O. Firstenberg, and I. Novikova, New J. Phys. **25**, 035001 (2023).
[5] A. K. Mohapatra, T. R. Jackson, and C. S. Adams, Phys. Rev. Lett. **98**, 113003 (2007).
[6] H. Kübler, J. P. Shaffer, T. Baluktsian, R. Löw, and T. Pfau, Nat. Photon. **4**, 112 (2010).
[7] N. Thaicharoen, K. R. Moore, D. A. Anderson, R. C. Powel, E. Peterson, and G. Raithel, Phys. Rev. A **100**, 063427 (2019).
[8] M. T. Simons, J. A. Gordon, and C. L. Holloway, Appl. Opt. **57**, 6456 (2018).
[9] J. A. Gordon, M. T. Simons, A. H. Haddab, and C. L. Holloway, AIP Adv. **9**, 045030 (2019).
[10] Y.-Y. Jau and T. Carter, Phys. Rev. Appl. **13**, 054034 (2020).
[11] C. T. Fancher, D. R. Scherer, M. C. S. John, and B. L. S. Marlow, IEEE Trans. Quantum Eng. **2**, 1 (2021).
[12] K. C. Cox, D. H. Meyer, F. K. Fatemi, and P. D. Kunz, Phys. Rev. Lett. **121**, 110502 (2018).
[13] N. Prajapati, A. P. Rotunno, S. Berweger, M. T. Simons, A. B. Artusio-Glimpse, S. D. Voran, and C. L. Holloway, AVS Quantum Science **4**, 035001 (2022).
[14] D. H. Meyer, P. D. Kunz, and K. C. Cox, Phys. Rev. Appl. **15**, 014053 (2021).
[15] C. L. Holloway, J. A. Gordon, A. Schwarzkopf, D. A. Anderson, S. A. Miller, N. Thaicharoen, and G. Raithel, Appl. Phys. Lett. **104**, 244102 (2014).
[16] L. A. Downes, A. R. MacKellar, D. J. Whiting, C. Bourgenot, C. S. Adams, and K. J. Weatherill, Phys. Rev. X **10**, 011027 (2020).
[17] L. A. Downes, L. Torralbo-Campo, and K. J. Weatherill, New J. Phys. **25**, 035002 (2023).
[18] C. L. Holloway, M. T. Simons, J. A. Gordon, A. Dienstfrey, D. A. Anderson, and G. Raithel, J. Appl. Phys. **121**, 233106 (2017).
[19] L. Ma, Electromagnetic field sensing with rydberg atoms in vapor cells, Ph.D. thesis, University of Michigan, 2021.
[20] M. Tanasittikosol, Rydberg dark states in external fields, Ph.D. thesis, Durham University, 2011.
[21] M. O. Scully and M. S. Zubairy, *Quantum Optics* (Cambridge University Press, Cambridge, 2001).
[22] T. Zanon, S. Guerandel, E. de Clercq, D. Holleville, N. Dimarcq, and A. Clairon, Phys. Rev. Lett. **94**, 193002 (2005).
[23] M. Abdel Hafiz, G. Coget, P. Yun, S. Guérandel, E. de Clercq, and R. Boudot, J. Appl. Phys. **121**, 104903 (2017).
[24] J. R. Johansson, P. D. Nation, and F. Noriac, Comput. Phys. Commun. **184**, 1234 (2013).
[25] H. Failache, L. Lenci, and A. Lezama, Phys. Rev. A **81**, 023801 (2010).
[26] I. S. Radojičić, M. Radonjić, M. M. Lekić, Z. D. Grujić, D. Lukić, and B. Jelenković, J. Opt. Soc. Am. B **32**, 426 (2015).
[27] R. M. Jenkins, E. E. Mikhailov, and I. Novikova, J. Opt. Soc. Am. B **36**, 890 (2019).